minerals

MDPI

Article

Involvement of Evaporite Layers in the Formation of Iron Oxide-Apatite Ore Deposits: Examples from the Luohe Deposit in China and the El Laco Deposit in Chile

Dongwei Guo [1,2,*], Yanhe Li [1,*], Chao Duan [1] and Changfu Fan [1]

[1] Ministry of Natural Resources Key Laboratory of Metallogeny and Mineral Assessment, Institute of Mineral Resources, Chinese Academy of Geological Sciences, Beijing 100037, China
[2] School of Earth and Space Sciences, Peking University, Beijing 100871, China
* Correspondence: guodongwei@stu.pku.edu.cn (D.G.); lyh@cei.cn (Y.L.)

Abstract: Iron oxide-apatite (IOA) deposits are important sources of iron. The role of evaporite layers in the formation of IOA ore deposits remains controversial. The Luohe deposit in eastern China and the El Laco deposit in Chile are representative IOA deposits. In this study, the S isotope characteristics of these two deposits are revisited. The formation of the Luohe ore deposit is closely related to marine evaporite layers in the Middle Triassic Dongma'anshan Formation. At Luohe, most of the sulfides and sulfates have high $\delta^{34}S_{V\text{-}CDT}$ values (concentrated from 6‰ to 10‰ and 16‰ to 20‰, respectively). The $\delta^{34}S_{V\text{-}CDT}$ values of sulfates are similar to those of marine evaporite layers (28–30‰) in the Dongma'anshan Formation. Estimates show that 46–82% of sulfur in the Luohe deposit is derived from marine evaporite layers. Unlike the Luohe deposit, the El Laco ore deposit formed in close relation to terrestrial evaporite layers from the Cretaceous-Tertiary Salta Group. At El Laco, the sulfides and sulfates have lower $\delta^{34}S_{V\text{-}CDT}$ values of −2.3‰ to −0.9‰ and 6.8‰ to 10.5‰, respectively. The $\delta^{34}S_{V\text{-}CDT}$ values of sulfates from the El Laco deposit are similar to those of sulfates from terrestrial evaporite layers (9.5‰) in the Salta Group. Estimates reveal that more than 70% of sulfur comes from terrestrial evaporite layers. These results indicate that evaporite layers have been involved in IOA ore-forming systems of both hydrothermal and magmatic deposits. Evaporite layers are proposed to have played key roles in the ore-forming processes of the Luohe and the Laco deposits and in other IOA deposits elsewhere.

Keywords: iron oxide-apatite deposit; evaporite layers; sulfur isotopes; Luohe deposit; El Laco deposit

Citation: Guo, D.; Li, Y.; Duan, C.; Fan, C. Involvement of Evaporite Layers in the Formation of Iron Oxide-Apatite Ore Deposits: Examples from the Luohe Deposit in China and the El Laco Deposit in Chile. *Minerals* **2022**, *12*, 1043. https://doi.org/10.3390/min12081043

Academic Editor: Georgy Cherkashov

Received: 2 August 2022
Accepted: 18 August 2022
Published: 19 August 2022

1. Introduction

Iron oxide-apatite (IOA) deposits, also known as magnetite-apatite deposits or Kiruna-type deposits, are an important type of porphyrite Fe deposits that occurred sporadically over a considerable time span ranging from the Paleoproterozoic to the Pliocene; they are mainly found at convergent boundaries, such as the Kiruna and Grängesberg districts in Sweden, the Bafq and Zanjan districts in Iran, the Great Bear zone in Canada, the Adirondack and Missouri districts in the United States, the High Andes and iron belt in Chile, and the Ningwu and Luzong districts in eastern China [1–22]. IOA deposits are characterized by massive and disseminated magnetite-apatite ± actinolite ores with Na, Ca, and K alteration and have a close spatial relationship with evaporite layers [2,4,18,23–29], which dominantly comprise gypsum/anhydrite, halite, and carbonates [2,30–33]. However, whether the evaporite layers are involved and play an important role in the formation of IOA ore deposits remains controversial. As the most important oxidation barrier, assimilation of evaporate layers played a key role in the formation of IOA deposits [2,4,14,18,23,26,28,29], while other researchers argue that evaporate layers are not needed to form IOA deposits [13].

The Luohe deposit in eastern China and the El Laco deposit in northern Chile are two typical IOA deposits. The Luohe deposit has been described as a hydrothermal IOA deposit

comprising massive, disseminated, and vein-type magnetite-apatite-diopside/actinolite ores, with widespread anhydrite-diopside alteration [34–38]. At Luohe, marine evaporite layers appear in the mining area and have a close spatial relationship with ore bodies [4,39]. The El Laco deposit is the youngest and best-preserved IOA deposit in the world and contains typical magmatic Fe ores [40–43], with terrestrial evaporite layers occurring in the region [44–46]. Sulfur isotopes are sensitive tracers of sulfur sources and ore-forming processes [47–50]. In this study, the published sulfur isotope data of these two deposits are reviewed and revisited. The proportions of sulfur from the evaporate layers in the two deposits are calculated and discussed to reveal the involvement of evaporite layers and provide new insights for understanding the formation of IOA deposits.

2. Deposit Geology

2.1. Luohe Deposit

The Luohe deposit is located in the western part of the Luzong ore district, which is one of the major Fe ore districts in eastern China (Figure 1). The strata of the Luzong ore district can be divided into three parts: (1) pre-Sinian metamorphic basement; (2) Sinian to Early Triassic marine clastic and carbonate rocks; and (3) Middle-Late Triassic to Cretaceous terrigenous clastic and volcanic rocks [36,51,52]. In the Early Cretaceous (135−127 Ma) [53], intense volcanism developed, producing the Longmenyuan, Zhuanqiao, Shuangmiao, and Fushan Formations. The IOA deposits are related to intrusions that occurred in the late depositional interval of the volcanic Zhuanqiao Formation [35] at ca. 130 Ma [39,54–56].

At the Luohe deposit, lime dolomite, breccia limestone and anhydrite limestone of the Middle Triassic Dongma'anshan Formation, trachyandensite and volcaniclastic rocks of the Zhuanqiao Formation, and basaltic trachyandesite of the Shuangmiao Formation occur in the mining area [13,34,57–59]. There are three types of ores. Anhydrite ores occur in the upper part, while pyrite ores and magnetite ores occur in the middle and lower parts [34]. The Fe ore bodies are distributed in the volcanic rocks of the Zhuanqiao Formation, with bedded and lenticular structures (Figure 2).

There are three vertical alteration/mineralization zones from top to bottom: (1) an upper, light-colored zone consists of silicate, kaolinite, chlorite-epidote, alunite, and anhydrate alteration with pyrite mineralization with a thickness of 400 m; (2) a middle, dark-colored zone consisting of diopside–garnet, chlorite–epidote, scapolite alteration, and Fe ores represents the main mineralization zone and has thicknesses of 300–500 m; and (3) a lower, light-colored zone is characterized by strong alkaline alteration consisting of major albite or K-feldspar alteration with retrograde alteration to sericite, carbonates, zeolites, and pyrite, with thicknesses of 250–300 m [18]. The main ore types include vein, veinlet, massive and disseminated types. Magnetite is one of the most important metallic minerals in the deposit, with a prevalent assemblage of diopside–magnate–apatite, which can be divided into disseminated and veined occurrences (Figure 3A). Pyrite ores are usually formed after the crystallization of magnetite, mainly comprising anhydrite–pyrite, magnetite–pyrite and anhydrite–pyroxene–pyrite assemblages (Figure 3B,C). Anhydrite is distributed widely, occurring mainly in the middle and upper alteration zones, some of which form anhydrite ore bodies (Figure 3D).

In addition, the Xiaobaozhuang skarn iron deposit has been found underneath the Luohe deposit, near the contact zone between trachyandensite of the Zhuanqiao Formation and evaporite layers of the Dongma'anshan Formation; this skarn deposit shows features similar to those of the Luohe deposit (Figure 4).

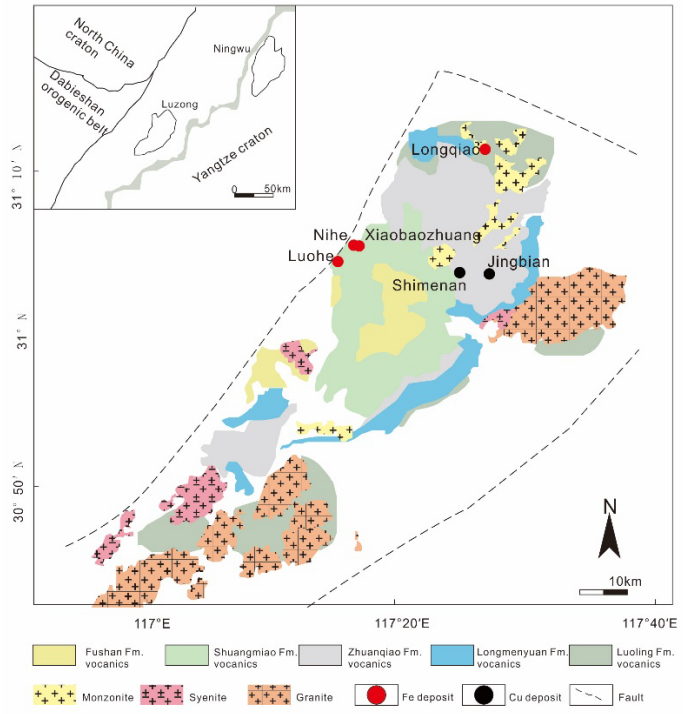

Figure 1. Geological map of the Luzong ore district (after [55]).

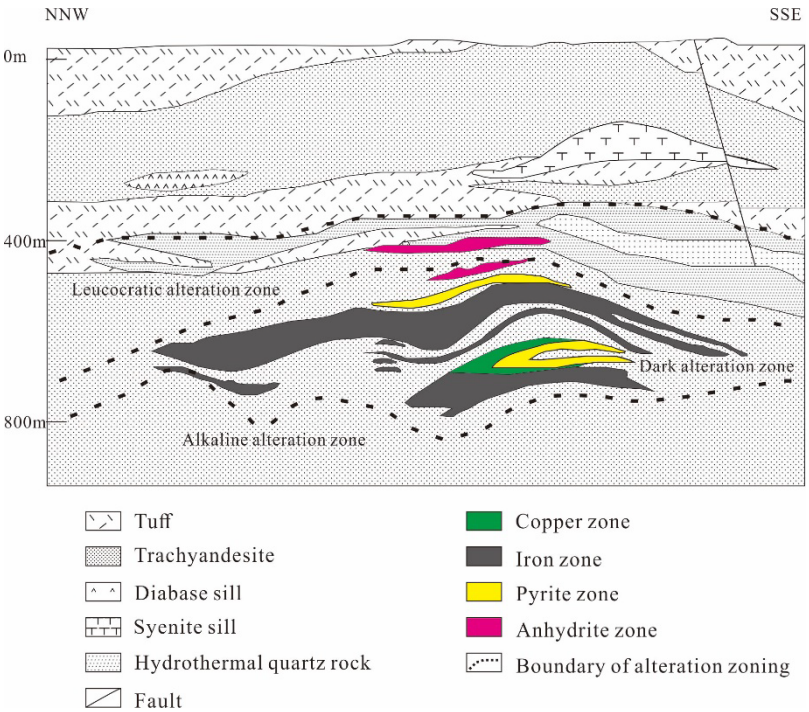

Figure 2. Section of the Luohe IOA deposit with mineralization and alteration zones (modified from [60]).

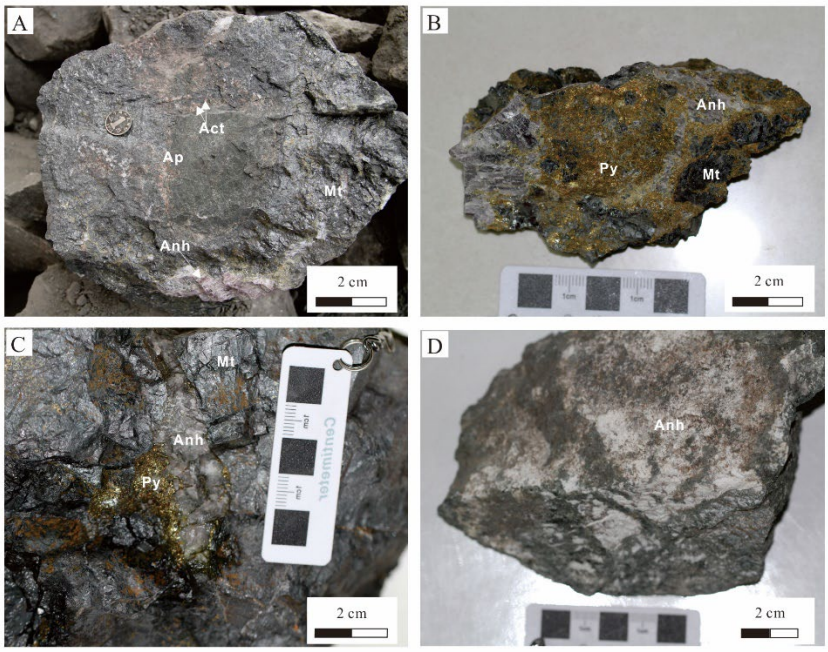

Figure 3. Photographs of Fe ore textures in the Luohe deposit. (**A**) Breccia apatite–magnetite–actinolite ore, with coarse-grained purple gypsum and sporadic apatite and actinolite. (**B**) Disseminated pyrite in magnetite ore with anhydrite. (**C**) Iron ore with anhydrite and pyrite replacements. (**D**) Anhydrite ore. Abbreviations: Anh = anhydrite; Mt = magnetite; Py = pyrite; Ap = apatite; Act = actinolite.

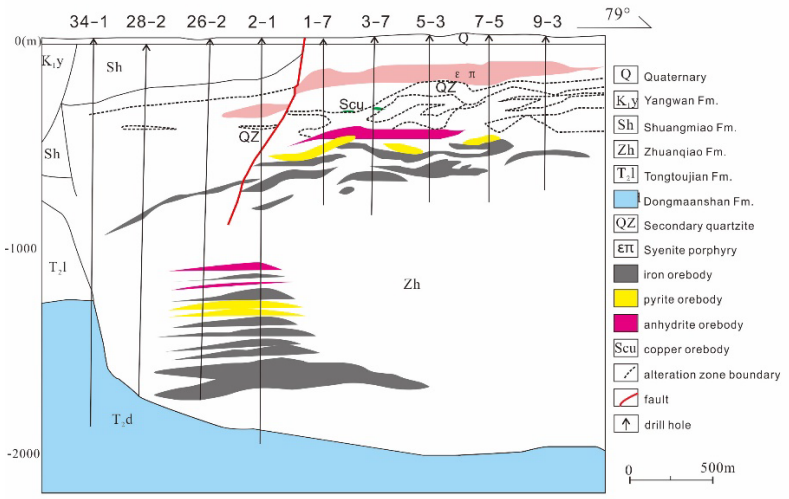

Figure 4. Geological section of the No. 3 prospecting line in the Luohe-Xiaobaozhuang system (after [37,61]).

2.2. El Laco Deposit

The El Laco IOA deposit is located on the Pune Plateau of the Andes in northern Chile on the slope of the Pliocene El Laco stratovolcano (5.3−1.6 Ma [62]), which consists of typical andesite flows (Figure 5) [63,64]. The El Laco deposit is underlain by thick sedimentary sequences, including limestones and sulfate evaporites of the Salta Group with a total thickness of 5000 m [31,44,64] and phosphatic siderite ironstones in the Paleozoic basement [43,65]. The Salta Group can be divided into three main units from base to top: (1) the Middle Cretaceous Pirgua Subgroup [66], which is composed of red beds; (2) the Maastrichtian to early Paleocene Balbuena Subgroup, which is composed of white sandstones (Lecho Formation), gray limestones with some layers of anhydrite and gypsum

(Yacoraite Formation) and dark pelites (Olmedo/Tunal Formations); and (3) the Paleogene Santa Barbara Subgroup, which is dominated by red fine-grained sandstone and siltstone and green mudstone. Several sulfate-rich units of the Yacoraite Formation are exposed to the east and west of the complex and likely extend laterally beneath El Laco [44,46]. The IOA deposits are closely related to the Yacoraite Formation, which formed in a carbonate shallow sea to hypersaline lake environment and is mainly composed of limestone and sandstone [31,64].

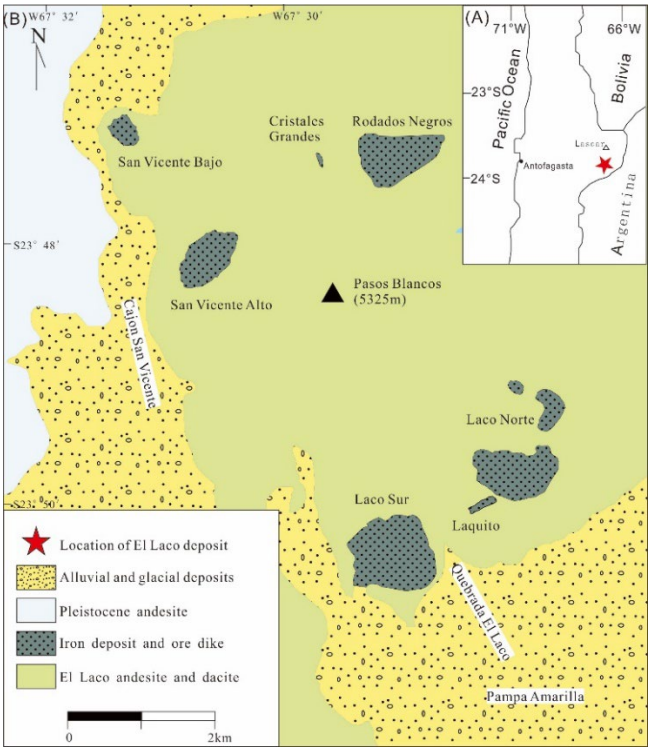

Figure 5. Location (**A**) and regional geologic setting (**B**) of the El Laco deposit in Chile (modified from [62]).

The magmatic rocks in the El Laco deposit are mainly composed of andesite, ignimbrite, pyroclastic andesite, dacite, and rhyolite and covered by Quaternary fluvial sediments in Quaternary (Figure 5B) [62,67]. The ore bodies crop out around the El Laco volcanic plug. Most mineralization occurs as strata-bound ore bodies interbedded with andesite flows or subvertical veins [63,64], forming the two large Laco Norte and Laco Sur ore bodies, with four other smaller ore bodies (Cristales Grandes, Rodados Negros, San Vicente Alto, and San Vicente Bajo). The ore bodies show prominent volcanic features, including flow banding, pipe vesicles, pahoehoe texture, and columnar jointing (Figure 6A,B) [63,64,68,69].

The alteration can be divided into three vertical zones from bottom to top: (1) an earlier, deep zone of Na-Ca alteration; (2) a dominant K-Ca alteration assemblage with diopside, magnetite, scapolite, pyroxene, garnet, apatite and anhydrate and small amounts of pyrite and chalcopyrite mineralization; and (3) a later, shallow zone of acid-sulfate alteration, characterized by abundant gypsum, montmorillonite, kaolinite, alunite, quartz and hematite, together with deposition of sulfides (Figure 6C) [64]. Vast quantities of anhydrite and gypsum occur as stockwork veins, mounds, and sulfate-rich zones in the shallow zone of acid-sulfate alteration (Figure 6D) [64].

A brief comparison of geological characteristics between the Luohe IOA deposit in eastern China and the El Laco IOA deposit in Chile is shown in Table 1.

Table 1. A brief comparison of geological characteristics from Luohe and El Laco IOA deposits.

Geological Characteristics \ Deposits	Luohe	El Laco
Host rock	Trachyandesite and diorite porphyrite	Andesite and rhyolite
Evaporite layers	Marine evaporite layers of the Dongma'anshan Formation	Terrestrial evaporite layers of the Salta Group
Ore-controlling structure	Rock fissures and fractures near contact zone	Diatreme
Ore body	Nearly bedded and lenticular shapes	Stratified upper part and lower part with vertical veins and domes
Ore structures	Veined, net-veined, disseminated, breccia and massive structures	Massive, vesicular, lava flows, skeleton and columnar structures
Essential minerals	Mag, (Hem), Py, Ccp, Ab, Kfs, Di, Grt, Ap, Wo, Anh, Chl, Cal, Qz	Mag, (Hem), Di, Scp, Ap, Kfs, Anh, Act
Alteration	Deep dark zone with skarn and anhydrite pyroxene alteration and shallow light zone with silicate and kaolinite alteration	Seep alkali-calcic alteration and shallow acid-sulfate alteration
Main metallogenic age	131.0–129.1 Ma	(5.3 ± 1.9)–(1.6 ± 0.5) Ma (host volcanic rock)
Fluid temperature and salinity in early mineralization	>830 °C, ~90% NaCl eq	>900 °C (Magnetite–diopside oxygen isotope temperature); 40%–60% NaCl eq
References	[4,58]	[42,64,70,71]

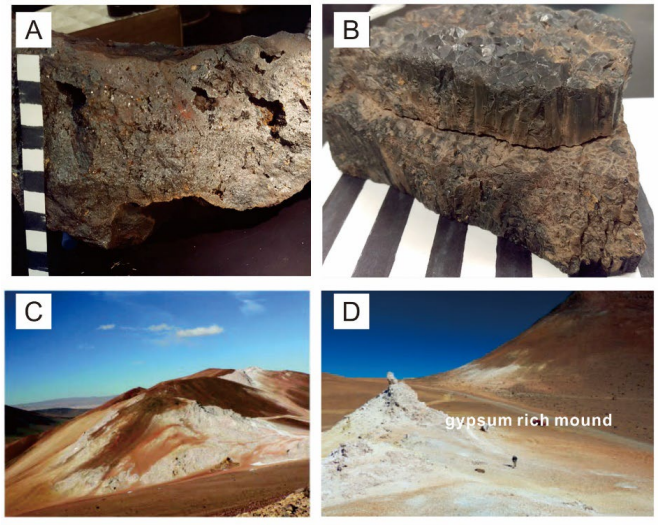

Figure 6. Photographs of geological features in the El Laco deposit. (**A**) Highly vesicular and oxidized magnetite from San Vicente Alto. (**B**) Columnar magnetite from Rodados Negros. (**C**) Large zones of acid-sulfate alteration in Laco Norte. (**D**) Gypsum-rich mound in the zone of acid-sulfate alteration, consisting of gypsum with minor cristobalite and alunite, at Pasos Blancos (after [64,68]).

3. Discussion

3.1. Sulfur Source

Sulfur isotopes can provide important constraints on the origin of sulfur in ore deposits [47,50,72]. Sulfide (pyrite) and sulfates (gypsum/anhydrite), with unique diopside–

gypsum–magnetite (gypsum–pyroxene) and garnet–gypsum–magnetite assemblages, are developed in the Luohe and El Laco IOA deposits [2,4,18,38,64,73]. The relative ^{34}S enrichment in sulfates is much larger than that in sulfides [72]. If the sulfur in deposits is mainly derived from magma, the $\delta^{34}S_{V\text{-}CDT}$ value of the total sulfur is approximately 0. Based on mass balance calculations, the $\delta^{34}S_{V\text{-}CDT}$ values of sulfides should be significantly negative in the presence of widespread sulfates and magnetite (or hematite) [74]. On the other hand, if the sulfur comes mainly from evaporite layers, the $\delta^{34}S_{V\text{-}CDT}$ values of sulfides should be higher in the high-temperature mineralization system.

3.1.1. Luohe Deposit

The sulfur isotope compositions of pyrite and gypsum at Luohe are shown in Table 2 [18,38,61,73,75]. The results yield a range of $\delta^{34}S_{V\text{-}CDT}$ values from −14.0‰ to 11.1‰ (n = 174, average of 4.2) for pyrite and 13.6‰ to 24.4‰ (n = 126, average of 18.1) for anhydrite. The pyrite and anhydrite $\delta^{34}S_{V\text{-}CDT}$ values are concentrated at 6‰ to 10‰ and 16‰ to 20‰, respectively (Figure 7). The sulfur isotope compositions of the Luohe deposit and evaporite layers show the following trends. (1) The pyrite $\delta^{34}S_{V\text{-}CDT}$ values are markedly positive, higher than that of mantle-derived magma and lower than that of anhydrite in the ore body. (2) All anhydrite in the ore body is significantly enriched in ^{34}S relative to pyrite, and the $\delta^{34}S_{V\text{-}CDT}$ values are similar to those of anhydrite from the evaporite layers (n = 3, average of 29.7‰) in the Dongma'anshan Formation near the ore district [18]. Therefore, sulfur in the Luohe IOA deposit is probably sourced from a mixture of primitive magma and evaporite layers.

Table 2. Sulfur isotope compositions of pyrite and gypsum in the Luohe and El Laco IOA deposits and gypsum from evaporite layers near the deposits.

Deposits/ Evaporite Layers		$\delta^{34}S_{V\text{-}CDT}$ (‰) of Pyrite		$\delta^{34}S_{V\text{-}CDT}$ (‰) of Gypsum		$\Delta^{34}S_{SO4\text{-}S2\text{-}}$ (‰)	References
		Variation Range	Average	Variation Range	Average		
Luohe	deposit	−14.0–11.1	4.2 (174)	13.6–24.4	18.1 (126)	13.9	[61,73,75]; this study
Xiaobaozhuang	deposit	6.9–14.2	10.8 (17)	16.4–32.2	23.3 (17)	12.5	[38]
El Laco	deposit	−2.3–0.9	−1.8 (4)	6.8–10.5	8.45 (8)	10.25	[64,76]
Dongma'anshan Formation	evaporite layers			29.4–29.9	29.7 (3)		[18]
Salta Group	evaporite layers			4.9–14.1	9.5 (12)		[76]

The $\delta^{34}S_{V\text{-}CDT}$ values of pyrite in the Luohe IOA deposits vary widely. The $\delta^{34}S_{V\text{-}CDT}$ values of pyrite in the magnetite mineralization stage are higher than those of pyrite in the sulfide stage [77]. The $\delta^{34}S_{V\text{-}CDT}$ values of pyrite in the Luohe deposit gradually decrease from deep to shallow levels, but the $\delta^{34}S_{V\text{-}CDT}$ values of anhydrite are relatively stable (Figure 8) [34,77]. These results indicate that sulfate plays a dominant role in this sulfur-containing magmatic–hydrothermal ore-forming system and governs the stable $\delta^{34}S_{V\text{-}CDT}$ values of sulfates, while the changes in sulfur isotopes in pyrite are mainly controlled by the sulfide-sulfate mineral equilibrium temperature [32,61,77]. Based on the calculated isotopic fractionation factors between sulfide and sulfate (Table 2), the sulfide-sulfate equilibrium temperatures are approximately 720–770 °C and 750–810 °C in the Luohe and Xiaobaozhuang deposits, respectively [74]. The mineralization temperature gradually decreases from deep to shallow levels, leading to decreases in the $\delta^{34}S_{V\text{-}CDT}$ values of sulfides. The evaporite layers with high $\delta^{34}S_{V\text{-}CDT}$ values are the main sulfur source endmember for the deposit.

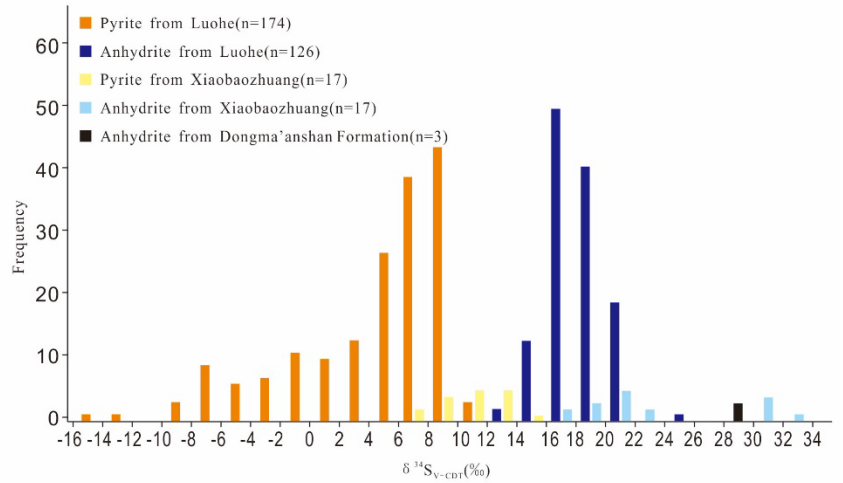

Figure 7. Sulfur isotope compositions of pyrite and anhydrite in the Luohe deposit and gypsum in the Dongma'anshan Formation near the Luohe deposit (data are listed in the Table S1 and obtained from [18,38,61,73,75]).

The origin of sulfur can be discussed on the basis of the isotopic composition of total sulfur. In the region of high fO_2 where sulfate species are significant, $\delta^{34}S_{sulfate} \approx \delta^{34}S_{\sum S}$ [72,74]. Therefore, the sulfur isotope value of sulfate represents the sulfur isotope characteristic of total sulfur in the ore-forming fluid [61,77]. Assuming the $\delta^{34}S_{V\text{-}CDT}$ value of the original magmatic sulfur to be 0‰ and the $\delta^{34}S_{V\text{-}CDT}$ value of the evaporite layers to be 29.7‰ [18], according to the $\delta^{34}S_{V\text{-}CDT}$ values of sulfates in the Luohe deposit (from 13.6‰ to 24.4‰) [61,73,75] and binary mixing calculations (Equation (1)), an estimated 46%–82% of the sulfur in the Luohe deposit comes from the evaporite layers in the Dongma'anshan Formation.

$$\delta^{34}S_{\sum S} = \delta^{34}S_{magma} \times X_1 + \delta^{34}S_{evaporite\ layers} \times (1 - X_1) \quad (1)$$

X_1, $1-X_1$ are proportions of sulfur from the magma and evaporate layers, respectively.

The Xiaobaozhuang deposit is located underneath the Luohe deposit. Note that pyrite and anhydrite from the deeper deposit have higher $\delta^{34}S_{V\text{-}CDT}$ values than those from the Luohe deposit. The $\delta^{34}S_{V\text{-}CDT}$ values of pyrite decrease vertically from bottom to top, ranging from 6.9‰ to 14.2‰, and $\delta^{34}S_{V\text{-}CDT}$ values of anhydrite are relatively stable at approximately 20‰ (Figure 8) [38,73], indicating that the mineralization temperature gradually decreases from deep to shallow levels and that the sulfur in the Xiaobaozhuang deposit also comes mainly from evaporite layers in the Dongma'anshan Formation.

3.1.2. El Laco Deposit

As shown in Table 2 and Figure 9, most of the $\delta^{34}S_{V\text{-}CDT}$ values of pyrite in the El Laco deposit are near zero, ranging from −2.3‰ to −0.9‰ (n = 4) [64]. However, the average $\delta^{34}S_{V\text{-}CDT}$ value of anhydrite is 8.45‰, with a narrow range from 6.8‰ to 10.5‰ (n = 8) [64], which is similar to that of sulfates from the evaporite layers in the Salta Group (average of 9.5‰, n = 12) [64,76]. Therefore, a possible source of sulfur for the ^{34}S-enriched anhydrite would be the evaporite layers in the Salta Group.

The El Laco deposit has widespread gypsum and includes some assemblages accompanied by large amounts of anhydrite and minor pyrite or chalcopyrite, indicating that sulfates also play a dominant role in the sulfide-sulfate system and that the sulfur isotope values of sulfates (from 6.8‰ to 10.5‰) represent the sulfur isotope characteristics of total sulfur in the ore-forming fluid [72,74]. According to the sulfate $\delta^{34}S_{V\text{-}CDT}$ values in the El Laco deposit and binary mixing calculations (Equation (1)), more than 70% of the sulfur is estimated to originate from the evaporite layers of the Salta Group by assuming the

$\delta^{34}S_{V\text{-}CDT}$ value of primitive magmatic sulfur to be 0‰ and the $\delta^{34}S_{V\text{-}CDT}$ value of sulfates in evaporite layers from the Salta Group to be 9.5‰.

According to the equilibrium equation and the relative sulfur isotope enrichment factor between sulfate and sulfide (Table 2) [74], the calculated sulfate-sulfide equilibrium temperature is almost 820–900 °C. These results indicate that S^{2-} and SO_4^{2-} could have formed at high temperatures when magmas assimilated and mixed with evaporite layers during magmatic ascent. Meanwhile, the El Laco deposit could likely be a magmatic–hydrothermal system in which the involvement of evaporite layers played a key role.

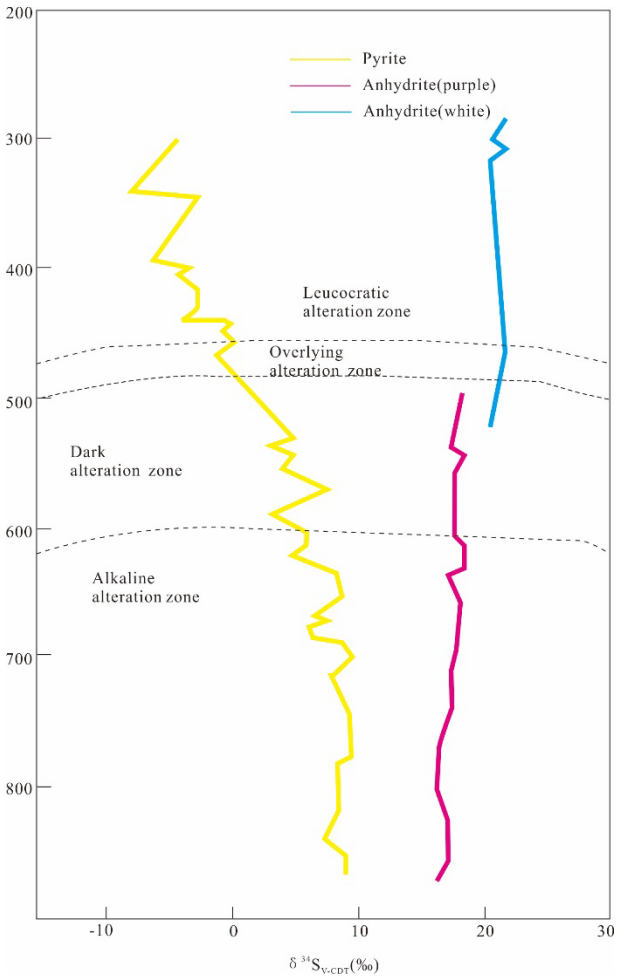

Figure 8. Variation in sulfur isotope characteristics with depth in the Luohe deposit in eastern China (after [61]).

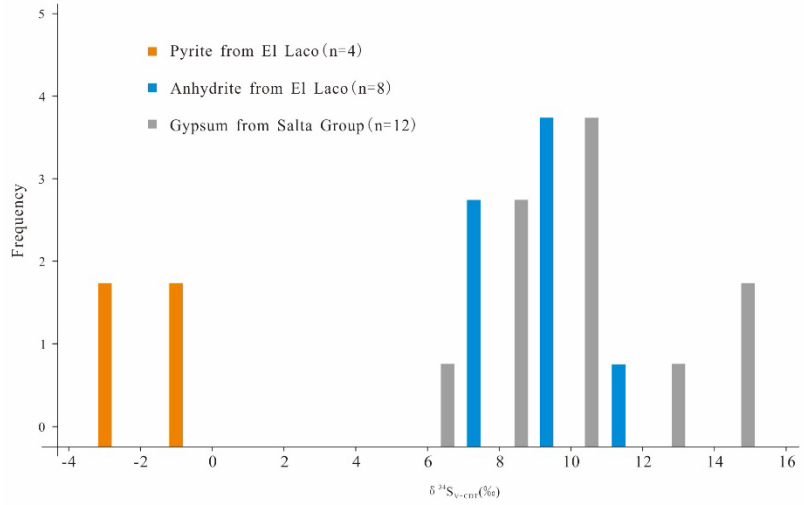

Figure 9. Sulfur isotope compositions of pyrite and anhydrite in the El Laco deposit and gypsum from the Salta Group (data are listed in the Table S1 and obtained from [64,76]).

In summary, the sulfur isotope composition of total sulfur in the ore-forming fluid within the magmatic–hydrothermal system depends on the sulfur source, and is strongly controlled by physicochemical conditions, including temperature, fO_2 and pH [2,32,47,72,77]. As mentioned above, the calculated proportion of sulfur from the evaporite layers shows that these layers are involved in the ore-forming process at both the Luohe and El Laco IOA deposits. The difference is that the sulfur in the Luohe deposit is mainly sourced from marine evaporite layers, while the sulfur in the El Laco deposit mostly originates from terrestrial evaporite layers. The $\delta^{34}S_{V\text{-}CDT}$ values of sulfates from terrestrial evaporite layers are lower than those of marine evaporite layers, resulting in lower $\delta^{34}S_{V\text{-}CDT}$ values of sulfate and sulfide minerals in the El Laco IOA deposits. It is reasonable to conclude that sulfur is derived only from magma when $\delta^{34}S_{V\text{-}CDT}$ values of total sulfur are near zero in the mineralization system. However, $\delta^{34}S_{V\text{-}CDT}$ values of sulfides do not represent the sulfur isotope composition of total sulfur in the presence of widespread sulfates and Fe-oxides. Under the conditions of large-scale sulfates and Fe-oxides, if magmatic sulfur is the signal sulfur source in the deposits, $\delta^{34}S_{\sum S} \approx 0$ and $\delta^{34}S_{V\text{-}CDT}$ values of sulfides will be significantly negative rather than 0. On the other hand, if $\delta^{34}S_{V\text{-}CDT}$ values of sulfides are near zero, $\delta^{34}S_{V\text{-}CDT}$ values of total sulfur will be markedly positive. Therefore, the sulfur source in the deposit cannot be determined simply based on the $\delta^{34}S_{V\text{-}CDT}$ values of sulfides. The physicochemical conditions and the geological and geochemical characteristics, especially whether sulfates and iron oxides exist on a large scale, need to be considered when applying the sulfur isotopes in tracing ore-forming material sources of IOA deposits.

3.2. The Participation of Evaporite Layers in the Process of Mineralization

As mentioned above, the evaporite layers are significantly involved in ore formation at both the Luohe and El Laco IOA deposits. Questioning when involvement occurs is logical.

Li et al. (2015) [4] found fluid inclusions in garnet that formed at the stage before the main mineralization and contain various daughter crystals such as anhydrite and halite; these observations are quite consistent with the widespread albite and scapolite alteration in the early mineralization within the Luohe deposit. The same authors also found that the initial fluids are high-temperature (~780 °C and hypersaline (~90 wt.% $NaCl_{eq}$) fluids with high oxygen fugacity. Fluid and melt inclusions, especially the earliest and most primitive melt inclusions, are valuable features that record the origin and evolution of ore-forming fluids [78]. The compositions of fluid and melt inclusions imply that fluids evolved from magmas and assimilated substantial amounts of evaporite layers during magmatic ascent

and that the involvement of evaporite layers might have started in the initial stages of Fe mineralization.

The involvement of evaporite layers in the mineralization system from the initial ore-formation stage is also supported by the carbonate-sulfate Fe-rich fluid and melt inclusions reported in the El Laco deposit in Chile; the Buena Vista and Iron Springs deposits in the United States; and the Meishan, Nihe and Luohe IOA deposits in eastern China [4,29,79]. Moreover, igneous rocks associated with El Laco IOA systems show direct evidence of the assimilation of evaporite layers in the form of sedimentary xenoliths from the Yacoraite Formation [44].

The addition of evaporite layers (rich in Na^+, K^+, Ca^{2+}, Cl^-, $CO_3{}^{2-}$, $SO_4{}^{2-}$ and H_2O) into an Fe-bearing magma is considered to be a key factor in IOA ore formation [3,4,14,17,18,26,32]. Evaporite layers are important oxidation barriers that can oxidize Fe^{2+} in the silicate melt to Fe^{3+} and prevent Fe from entering the lattice of Fe-rich silicate minerals such as pyroxene and amphibole, forming Fe-poor diopside and tremolite, while Fe oxides enter the melt (as shown in Equations (2) and (3)). This is proven by the large-scale anhydrite–diopside and actinolite/tremolite alteration in the Ningwu and Luzong districts and the extensive development of diopside alteration and anhydrite alteration and iron ore magma in the El Laco deposits in Chile [4,42].

$$FeMgSi_2O_6 + CaSO_4 \rightarrow CaMgSi_2O_6 + Fe_3O_4 + FeS_2 \quad (2)$$

$$Ca_2(Mg, Fe)_5[Si_4O_{11}](OH)_2 + CaSO_4 \rightarrow Ca_2Mg_5[Si_4O_{11}](OH)_2 + Fe_3O_4 + FeS_2 \quad (3)$$

On the other hand, evaporite layers could provide P, NaCl and volatiles, which would promote the occurrence of liquid immiscibility in magma, forming an Fe oxide-P-volatile-rich melt and a Si-rich melt [80–83]. These enrichment mechanisms of Fe for IOA deposits have been proven by many natural phenomena and laboratory simulation experiments [6,11,42,43,84–86]. Moreover, the addition of oxygen agents increases the oxygen fugacity of the magmatic system, leading to the formation of numerous Fe oxides above the solidification temperature of silicate liquids, which has been proven by previous experiments [87,88]. Furthermore, Fe-volatile-rich melt evolves to an iron ore magma and a high-temperature, high-salinity, iron-rich magmatic–hydrothermal fluid. During the magmatic–hydrothermal process, hydrothermal fluid can activate the evaporate layers and transfer materials to the upper part, leading to reprecipitation of gypsum/anhydrite [2,18].

In the hydrothermal stage, with the continuous pulsed addition of $SO_4{}^{2-}$, NaCl and H_2O from evaporite layers, Fe^{2+} is oxidized to promote hydrothermal Fe-oxide precipitation, $SO_4{}^{2-}$ itself is reduced to S^{2-}, and S^{2-} combines with Fe^{2+} to form hydrothermal Fe-sulfide ores (Equation (4)). Evaporite layers can provide large numbers of agents such as Na^+ and Cl^- and cause Fe^{2+} transport as complexes (e.g., Na-Fe-Cl), probably forming hydrothermal-type ores in the distal zone from the evaporite layers [32].

$$Fe^{2+} + SO_4{}^{2-} \rightarrow Fe_3O_4 + FeS_2 \quad (4)$$

The coexistence of Fe oxides, Fe sulfides and sulfate in different stages of one IOA deposit is often observed in the field. The close genetic relation of these ores is shown in Equations (2)–(4). In IOA deposits, magma-type and hydrothermal-type ore bodies coexist, showing a close vertical relationship in space where magma-type and skarn-like ores occur in the deep contact zone between intrusive rocks and evaporite layers. IOA-type and hydrothermal–metasomatic-type ores are located in the shallow part in intrusive rock-related mineralization [2,32]. This is consistent with the Luohe IOA ores hosted in the upper part in intrusions and Xiaobaozhuang skarn Fe ores in the deeper part of the contact zone between intrusions and evaporites in this study. Therefore, Fe-oxide ores, Fe-sulfide ores and sulfate ores have a close spatial relationship and are potential prospecting indicators for each other in IOA deposits controlled by evaporite layers.

4. Conclusions

Evaporite layers were involved in the ore-forming process at both the Luohe and El Laco IOA deposits in the early mineralization stage. As the most important oxidation barrier, evaporite layers are a critical factor in the formation of an IOA ore deposit. The difference is that the sulfur in the Luohe deposit is derived mainly from marine evaporite layers, while the sulfur in the El Laco deposit mostly originates from terrestrial evaporite layers, resulting in higher $\delta^{34}S_{V\text{-}CDT}$ values of sulfate/sulfide in the Luohe deposit but lower $\delta^{34}S_{V\text{-}CDT}$ values in the El Laco deposit. It is unreasonable to conclude that sulfur is sourced only from magma based on the $\delta^{34}S_{V\text{-}CDT}$ values (~0‰) of sulfides (e.g., El Laco deposit) and to ignore the involvement of evaporite layers. This study highlights that evaporite layers are involved in the ore-forming process of IOA deposits related to both marine and terrestrial evaporite layers. This implies that IOA ores and Fe-sulfide ores have an intrinsic genetic relationship and belong to the same Fe mineralization system.

Supplementary Materials: The following supporting information can be downloaded at: https://www.mdpi.com/article/10.3390/min12081043/s1, Table S1: Sulfur isotope values of pyrite and sulfate from the Luohe and El Laco IOA deposits, and anhydrite from the Dongma'anshan Formation and Salta Group.

Author Contributions: Data curation, D.G. and Y.L.; Formal analysis, C.F.; Funding acquisition, Y.L. and C.D.; Writing—original draft, D.G.; Writing—review and editing, Y.L. and C.D. All authors have read and agreed to the published version of the manuscript.

Funding: This study was jointly supported by the National Natural Science Foundation of China (No. 41973022, 41627802 and 42172102) and Central Public-interest Scientific Institution Basal Research Fund (No. KK2015).

Acknowledgments: We gratefully thank two anonymous reviewers for their helpful comments and insightful reviews, which have greatly improved the manuscript.

Conflicts of Interest: The authors declare no conflict of interest.

References

1. Nabatian, G.; Ghaderi, M.; Corfu, F.; Neubauer, F.; Bernroider, M.; Prokofiev, V.; Honarmand, M. Geology, alteration, age, and origin of iron oxide–apatite deposits in upper eocene quartz monzonite, Zanjan district, NW Iran. *Miner. Depos.* **2013**, *49*, 217–234. [CrossRef]
2. Li, Y.-H.; Duan, C.; Han, D.; Chen, X.-W.; Wang, C.-L.; Yang, B.-Y.; Zhang, C.; Liu, F. Effect of sulfate evaporate salt layer for formation of porphyrite iron ores in the Middle-Lower Yangtze River area. *Acta Petrol. Sin.* **2014**, *30*, 1355–1368.
3. Zhang, S.; Wu, M.-A.; Zhao, W.-G.; Zhang, Y.-Y.; Li, X.-D.; Wang, J. Geochemistry characteristics of Nihe iron deposit in Lujiang, Anhui Province and their constrains to ore genesis. *Acta Petrol. Sin.* **2014**, *30*, 1382–1396.
4. Li, W.-T.; Audetat, A.; Zhang, J. The role of evaporites in the formation of magnetite–apatite deposits along the Middle and Lower Yangtze River, China: Evidence from LA-ICP-MS analysis of fluid inclusions. *Ore Geol. Rev.* **2015**, *67*, 264–278. [CrossRef]
5. Neymark, L.A.; Holm-Denoma, C.S.; Pietruszka, J.; Aleinikoff, N.; Fanning, C.M.; Pillers, R.M.; Moscati, R.J. High spatial resolution U-Pb geochronology and Pb Isotope geochemistry of magnetite-apatite ore from the Pea Ridge Iron Oxide-apatite deposit, St. Francois Mountains, Southeast Missouri, USA. *Econ. Geol.* **2016**, *111*, 1915–1933. [CrossRef]
6. Hou, T.; Charlier, B.; Namur, O.; Philip, S.; Ulrich, S.S.; Zhang, Z.-C.; Holtz, F. Experimental study of liquid immiscibility in the Kiruna-type Vergenoeg iron-fluorine deposit, South Africa. *Geochim. Cosmochim. Acta* **2017**, *203*, 303–322. [CrossRef]
7. Ootes, L.; Snyder, D.; Davis, W.J.; Acosta-Gongora, P.; Corriveau, L.; Mumin, A.H.; Gleeson, S.A.; Samson, I.M.; Montreuil, J.F.; Potter, E.; et al. A paleoproterozoic Andean-type iron oxide copper-gold environment, the Great Bear magmatic zone, Northwest Canada. *Ore Geol. Rev.* **2017**, *81*, 123–139. [CrossRef]
8. Zhang, Z.-Z.; Zhang, S.; Wu, M.-A.; Lv, B.; Wang, K.-Y.; Zhang, Q.-M. Geological characteristics and ^{40}Ar-^{39}Ar geochronology of Xiaobaozhuang iron deposit in Luzong volcanic basin. *Mineral Deposits.* **2017**, *36*, 795–815.
9. Heidarian, H.; Lentz, D.R.; Alirezaei, S.; McFarlane, C.R.M.; Peighambari, S. Multiple Stage Ore Formation in the Chadormalu Iron Deposit, Bafq Metallogenic Province, Central Iran: Evidence from BSE Imaging and Apatite EPMA and LA-ICP-MS U-Pb Geochronology. *Minerals* **2018**, *8*, 87. [CrossRef]
10. Palma, G.; Barra, F.; Reich, M.; Valencia, V.; Simon, A.C.; Vervoort, J.; Leisen, M.; Romero, R. Halogens, trace element concentrations, and Sr-Nd isotopes in apatite from iron oxide-apatite (IOA) deposits in the Chilean iron belt: Evidence for magmatic and hydrothermal stages of mineralization. *Geochim. Cosmochim. Acta* **2019**, *246*, 515–540. [CrossRef]

11. Xie, Q.-H.; Zhang, Z.-C.; Hou, T.; Cheng, Z.-G.; Campos, E.; Wang, Z.-C.; Fei, X.-H. New insights for the formation of Kiruna-type iron deposits by immiscible hydrous Fe-P melt and high-temperature hydrothermal processes: Evidence from El Laco deposit. *Econ. Geol.* **2019**, *114*, 35–46. [CrossRef]
12. La Cruz, N.L.; Ovalle, J.T.; Simon, A.C.; Konecke, B.A.; Barra, F.; Reich, M.; Leisen, M.; Childress, T.M. The geochemistry of magnetite and apatite from the el laco iron oxide-apatite deposit, Chile; implications for ore genesis. *Econ. Geol. Bull. Soc. Econo. Geol.* **2020**, *115*, 1461–1491. [CrossRef]
13. Liu, Y.-N.; Fan, Y.; Zhou, T.-F.; Fu, B.; Ireland, T.R.; Wang, J.-F.; Zhang, L.-J. Hydrothermal fluid characteristics and implications of the makou IOA deposit in Luzong basin, eastern China. *Ore Geol. Rev.* **2020**, *127*, 103867. [CrossRef]
14. Mao, J.-W.; Zhou, T.-F.; Xie, G.-Q.; Yuan, F.; Duan, C. Metallogeny in Middle-Lower Yangtze River ore belt: Advances and problems remained. *Min. Depos.* **2020**, *39*, 547–558.
15. Sadeghi, M.; Nikolaos, A.; Anna, L. Geochemistry of Rare Earth Elements in Bedrock and Till, Applied in the Context of Mineral Potential in Sweden. *Minerals* **2020**, *10*, 365. [CrossRef]
16. Yu, J.-J.; Chen, B.-Y.; Che, L.R.; Wang, T.Z.; Liu, S.-J.; Horvath, P. Genesis of the meishan iron oxide–apatite deposit in the ningwu basin, eastern China: Constraints from apatite chemistry. *Geol. J.* **2020**, *55*, 1450–1467. [CrossRef]
17. Zhao, X.-F.; Zeng, L.P.; Liao, W.; Li, W.-T.; Hu, H.; Li, J.-W. An overview of recent advances in porphyrite iron (iron oxide-apatite, IOA) deposits in the middle-lower Yangtze river valley metallogenic belt and its implication for ore genesis. *Di Xue Qian Yuan* **2020**, *27*, 197–217.
18. Duan, C.; Li, Y.-H.; Mao, J.-W.; Zhu, Q.-Q.; Xie, G.-Q.; Wan, Q.; Jian, W.; Hou, K.-J. The Role of Evaporite Layers in the Ore-Forming Processes of Iron Oxide-Apatite and Skarn Fe Deposits: Examples from the Middle-Lower Yangtze River Metallogenic Belt, East China. *Ore Geol. Rev.* **2021**, *138*, 104352. [CrossRef]
19. Liu, Y.-N.; Fan, Y.; Zhou, T.-F.; Yan, L.; Fu, B.; Wang, F.-Y.; Wang, J.-F. Trace element evolution of magnetite in iron oxide-apatite deposits: Case study of Daling deposit, eastern China. *Ore Geol. Rev.* **2022**, *144*, 104842. [CrossRef]
20. Parvaresh, D.M.; Malekzadeh, S.A.; Azimzadeh, A.M.; Karimpour, M.H.; Klötzli, U. Textures and Chemical Compositions of the Narm Iron Oxide-Apatite Deposit in Kuh-e-Sarhangi District (Central Iran): Insights into the Magmatic-Hydrothermal Mineralization. *Ore Geol. Rev.* **2022**, *141*, 104631. [CrossRef]
21. Yan, S.-C.; Liu, W. Rare earth elements in the iron-oxide apatite (IOA) deposit: Insights from apatite. *Int. Geol. Rev.* **2022**, *140*, 104599. [CrossRef]
22. Zeng, L.-P.; Zhao, X.-F.; Spandler, C.; Hu, H.; Hu, B.; Li, J.-W.; Hu, Y. Origin of high-Ti magnetite in magmatic-hydrothermal systems; evidence from iron oxide-apatite (IOA) deposits of eastern China. *Econ. Geol. Bull. Soc. Econo. Geol.* **2022**, *117*, 923–942.
23. Cai, B.-J. The relationship of gypsum salt beds with endogenic copper and iron. *Geochimica* **1980**, *9*, 193–199.
24. Fan, H.-Y.; Li, W.-D.; Wang, W. –B. On the relationship between the marine Triassic evaporate horizons and Cu(Au), Fe deposits in the Middle-Lower Yangtze area. *Volcanol. Miner. Resour.* **1995**, *16*, 32–41.
25. Hou, Z.-Q.; Yang, Z.-S.; Li, Y.-Q.; Zeng, P.-S.; Meng, Y.-F.; Xu, W.-Y.; Tian, S.-H. Large-scale migration of fluids towards foreland basins during collisional orogeny: Evidence from Triassic anhydrock sequences and regional alteration in Middle-Lower Yangtze area. *Miner. Depos.* **2004**, *23*, 310–326.
26. Zhou, T.-F.; Fan, Y.; Yuan, F.; Wu, M.-A.; Zhao, W.-G.; Qian, B.; Ma, L.; Wang, W.-C.; Liu, Y.-N.; White, N. The metallogenic model of Nihe iron deposit in Lu-Zong basin and genetic relationship between gypsum-salt layer and deposit. *Acta Geol. Sin.* **2014**, *88*, 562–573.
27. Martinsson, O.; BillstrÖm, K.; Broman, C.; Weihed, P.; Wanhainen, C. Metallogeny of the Northern Norrbotten Ore Province, northern Fennoscandian Shield with emphasis on IOCG and apatite-iron ore deposits. *Ore Geol. Rev.* **2016**, *78*, 447–492. [CrossRef]
28. Duan, C.; Li, Y.-H.; Mao, J.-W.; Wang, C.-L.; Yang, B.-Y.; Hou, K.-J.; Wang, Q.; Li, W. Study on the ore-forming process of the Heshangqiao IOA deposit in the Ningwu ore district: Insight from magnetite LA-ICP-MS in-situ analysis data. *Acta Petrol. Sin.* **2017**, *33*, 3471–3483.
29. Bain, W.M.; Steele-MacInnis, M.; Tornos, F.; Hanchar, J.M.; Creaser, E.C.; Pietruszka, D.K. Evidence for iron-rich sulfate melt during magnetite (-apatite) mineralization at El Laco. *Chile. J. Geology.* **2021**, *49*, 1044–1048. [CrossRef]
30. Warren, J.K. Evaporites, brines and base metals: What is an evaporite? Defining the rock matrix. *Aust. J. Earth Sci. Int. Geosci. J. Geol. Soc. Aust.* **1996**, *43*, 115–132. [CrossRef]
31. Li, Y.-H.; Duan, C.; Han, D.; Liu, F.; Wan, D.-F.; Wang, C.-Y. Oxygen isotopic discriminant marker of magmatic iron deposits: Ningwu porphyrite iron ore as an example. *Acta Geol. Sin.* **2017**, *33*, 3411–3421.
32. Li, Y.-H.; Xie, G.-Q.; Duan, C.; Han, D. Effect of sulfate evaporate salt layer over the formation of skarn-type iron ores. *Acta Geol. Sin.* **2013**, *87*, 1324–1334.
33. Yaremchuk, Y.; Hryniv, S.; Peryt, T.; Vovnyuk, S.; Meng, F.-W. Controls on Associations of Clay Minerals in Phanerozoic Evaporite Formations: An Overview. *Minerals* **2020**, *10*, 974. [CrossRef]
34. Huang, Q.-T. A brief discussion on geological characteristics of the Luohe iron deposit in Anhui province. *Miner. Depos.* **1984**, *4*, 9–19.
35. Wu, M.-A.; Wang, Q.-S.; Zheng, G.-W.; Cai, X.-M.; Yang, S.-X.; Di, Q.S. Discovery of the Nihe Iron Deposit in Lujiang, Anhui, and its Exploration Significance. *Acta Geol. Sin.* **2011**, *85*, 802–809.
36. He, D.-F.; Gao, C.-S.; Zhang, K.; Wang, Y.-M. Zoning features of wall rock alteration of the Xiaobaozhuang iron deposit in Lujiang County, Anhui Province. *Geol. Anhui* **2014**, *24*, 86–90.

37. Liu, Y.-N.; Fan, Y.; Gao, C.-S.; Zhang, Q.-M.; Zhang, L.-J. Geological characteristics of Xiaobaozhuang iron deposit in the Lu-Zong volcanic basin, the Middle-Lower Yangtze River Valley Metallogenic Belt. *Acta Petrol. Sin.* **2016**, *32*, 319–333.
38. Wen, B.-B.; Zhang, Z.-C.; Xie, Q.-H.; Cheng, Z.-G.; Fei, X.-H.; Li, Z.X. Geological Characteristics and Metallogenic Mechanism of the Xiaobaozhuang Iron Deposit and Their Genetic Relationship with the Luohe Iron Deposit in the Lujian-Zongyang Basin, Anhui Province. *Acta Geol. Sin.* **2018**, *92*, 1474–1492.
39. Zhou, T.-F.; Fan, Y.; Yuan, F.; Zhang, L.-J.; Qian, B.; Ma, L.; Yang, X.-F.; Cooke, D. Geochronology and significance of volcanic rocks in the Ning-Wu basin of China. *Sci. China* **2011**, *54*, 185–196. [CrossRef]
40. Richard, H.S.; David, R.B. New field evidence bearing on the origin of the El Laco magnetite deposit, northern Chile-a reply. *Econ. Geol. Bull. Soc. Econ. Geol.* **2003**, *98*, 1501–1502.
41. Nyström, J.O.; Billstrom, K.; Henriquez, F.; Fallick, A.E.; Naslund, H.R. Oxygen Isotope Composition of Magnetite in Iron Ores of the Kiruna Type in Chile and Sweden. *GFF* **2008**, *130*, 177–188. [CrossRef]
42. Tornos, F.; Velasco, F.; Hanchar, J. Iron oxide melts, magmatic magnetite, and superheated magmatic-hydrothermal systems: The El Laco Deposit, Chile. *Geology* **2016**, *44*, 427–430. [CrossRef]
43. Mungall, J.E.; Long, K.; Brenan, J.; Smythe, D.; Naslund, H.R. Immiscible shoshonitic and Fe-P-oxide melts preserved in unconsolidated tephra at El Laco volcano, Chile. *Geology* **2018**, *46*, 255–258. [CrossRef]
44. Matthews, S.J.; Marquillas, R.A.; Kemp, A.J.; Grange, F.K.; Gardeweg, M.C. Active skarn formation beneath Lascar Volcano, northern Chile: A petrographic and geochemical study of xenoliths in eruption products. *J. Metamorph. Geol.* **1996**, *14*, 509–530. [CrossRef]
45. Marquillas, R.A.; del Papa, C.; Sabino, I.F. Sedimentary Aspects and Paleoenvironmental Evolution of a Rift Basin: Salta Group (Cretaceous-Paleogene), Northwestern Argentina. *Int. J. Earth Sci. Geol. Rundsch.* **2005**, *94*, 94–113. [CrossRef]
46. Scheuber, E.; Mertmann, D.; Ege, H.; Silva-González, P.; Heubeck, C.; Reutter, K.-J.; Jacobshagen, V. Exhumation and basin development related to formation of the Central Andean Plateau, 21 °S. In *The Andes*; Springer: Berlin/Heidelberg, Germany, 2006; pp. 285–301.
47. Rye, R.O.; Ohmoto, H. Sulfur and Carbon Isotopes and Ore Genesis: A Review. *Econ. Geol. Bull. Soc. Econ. Geol.* **1974**, *69*, 826–842. [CrossRef]
48. Ohmoto, H. Stable Isotope Geochemistry of Ore Deposits. *Rev. Mineral.* **1986**, *16*, 491–559.
49. Seal, R.R. Sulfur isotope geochemistry of sulfide minerals (Review). *Rev. Mineral. Geochem.* **2006**, *61*, 633–677. [CrossRef]
50. Hoefs, J. *Stable Isotope Geochemistry*, 7th ed.; Springer: Berlin/Heidelberg, Germany, 2015; pp. 1–389.
51. Zhang, S.; Fan, Y.; Wu, M.-A.; Wang, K.-Y.; Zhao, W.-G.; Wei, G.-H. Characteristics of ore-forming fluids in Nihe iron deposit in Luzong volcanic basin, Anhui Province, China: Evidences from He-Ar-H-O isotopes. *Acta Petrol. Sin.* **2016**, *32*, 377–389.
52. Zhang, S.; Zhou, T.-F.; Wu, M.-A.; Zhang, Z.-Z.; Xue, H.-M.; Li, X.-D. Geochronolgy and petrological geochemistry of intrusions in the Lujiang-Zongyang basin in the mineralization belt of the Middle and Lower Reaches of Yangtze River by scientific drilling. *Acta Geol. Sin.* **2017**, *91*, 1483–1505.
53. Zhou, T.-F.; Fan, Y.; Yuan, F. Advances on petrogensis and metallogeny study of the mineralization belt of the Middle and Lower Reaches of the Yangtze River area. *Acta Petrol. Sin.* **2008**, *24*, 1665–1678.
54. Zhou, T.-F.; Fan, Y.; Yuan, F.; Lu, S.-M.; Shang, S.-G.; Cooke, D.; Meffre, S.; Zhao, G.-C. Geochronology of the volcanic rocks in the Lu-Zong (Lujiang-Zongyang) basin and its significance. *Sci. China* **2008**, *51*, 1470–1482. [CrossRef]
55. Zhou, T.-F.; Fan, Y.; Yuan, F.; Song, C.-Z.; Zhang, L.-J.; Qian, C.-C.; Lu, S.-M.; Cooke, D.R. Temporal-spatial framework of magmatic intrusions in Luzong volcanic basin in East China and their constrain to mineralization. *Acta Petrol. Sin.* **2010**, *26*, 2694–2714.
56. Fan, Y.; Liu, Y.-N.; Zhou, T.-F.; Zhang, L.-J.; Yuan, F.; Wang, W.-C. Geochronology of the Nihe deposit and in the Lu-Zong basin and its metallogenic significances. *Acta Petrol. Sin.* **2014**, *30*, 1369–1381.
57. Liu, Y.-N.; Fan, Y.; Zhou, T.-F.; Zhang, L.-J.; White, N.; Hong, H.-L.; Zhang, W. LA-ICP-MS titanite U-Pb dating and mineral chemistry of the Luohe magnetite-apatite (MA)-type deposit in the Lu-Zong volcanic basin, Eastern China. *Ore Geol. Rev.* **2018**, *92*, 284–296. [CrossRef]
58. Zhang, L.-J. Polymetallic Mineralization and Associated Magmatic and Volcanic Activity in the Luzong Basin. Ph.D. Thesis, Hefei University of Technology, Hefei, China, 2011.
59. Fan, Y.; Zhang, W.; Liu, Y.-N.; Zhou, T.-F.; Zhang, L.-J.; Chen, X.-F.; Hong, H.-L. Geochemical Characteristics of Chlorite in the Luohe Iron Deposit in the Middle-Lower Yangtze Metallogenic Belt, Eastern China. *Ore Geol. Rev.* **2021**, *133*, 104062. [CrossRef]
60. Chang, Y.-F.; Liu, X.-P.; Wu, Y.-C. *The Copper-Iron Belt of the Lower and Middle Reaches of the Changjiang River*; Geological Publishing House: Beijing, China, 1991; pp. 1–234.
61. Huang, Q.-T.; Yin, G.-P. *The Luohe Iron Deposit in Lujiang County, Anhui Province*; Geological Publishing House: Beijing, China, 1989; pp. 1–191.
62. Naranjo, J.A.; Henríquez, F.; Nyström, J.O. Subvolcanic contact metasomatism at El Laco Volcanic Complex, Central Andes. *Andean Geol.* **2010**, *37*, 110–120. [CrossRef]
63. Naslund, H.R.; Henríquez, F.; Nyström, J.O.; Vivallo, W.; Dobbs, F.M. Magmatic iron ores and associated mineralisation: Examples from the Chilean High Andes and Coastal Cordillera. *Aust. Miner. Found.* **2002**, *2*, 207–226.
64. Tornos, F.; Velasco, F.; Hanchar, J.M. The magmatic to magmatic-hydrothermal evolution of the El Laco deposit (Chile) and its implications for the genesis of magnetite-apatite deposits. *Econ. Geol. Bull. Soc. Econ. Geol.* **2017**, *112*, 1595–1628. [CrossRef]

65. Boso, M.-A.; Monaldi, C.R. Oolitic stratabound iron ores in the Silurian of Argentina and Bolivia. *Spec. Publ. Soc. Geol. Appl. Miner. Depos.* **1990**, *8*, 175–186.
66. Reyes, F.C.; Salfity, J.A. Consideraciones sobre la estratigrafía del Cretá cico (Subgrupo Pirgua) del noroeste argentino. *Actas De Las Jorn. Geol. Argent.* **1973**, *3*, 355–385.
67. Kay, S.M.; Coira, B.L. Shallowing and steepening subduction zones, continental lithospheric loss, magmatism and crustal flow under the Central Alpiplano-Puna plateau. *Geol. Soc. Am. Bull.* **2009**, *204*, 229–259.
68. Childress, T.; Simon, A.C.; Reich, M.; Barra, F.; Bilenker, L.D.; Cruz, N.L.L.; Bindeman, I.N.; Ovalle., J.T. Triple Oxygen ($\delta^{18}O$, $\Delta^{17}O$), Hydrogen ($\delta^{2}H$), and Iron ($\delta^{56}Fe$) Stable Isotope Signatures Indicate a Silicate Magma Source and Magmatic-Hydrothermal Genesis for Magnetite Orebodies at El Laco, Chile. *Econ. Geol. Bull. Soc. Econ. Geol.* **2020**, *115*, 1519–1536. [CrossRef]
69. Nyström, J.O.; Henriquez, F.; Naranjo, J.A.; Naslun, H.R. Magnetite Spherules in Pyroclastic Iron Ore at El Laco, Chile. *Am. Mineral.* **2016**, *101*, 587–595. [CrossRef]
70. Nyström, J.O.; Henriquez, F. Magmatic features of iron ores of the Kiruna type in Chile and Sweden: Ore textures and magnetite geochemistry. *Econ. Geol. Bull. Soc. Econ. Geol.* **1994**, *89*, 820–839. [CrossRef]
71. Broman, C.; Nyström, J.O.; Henríquez, F.; Elfman, M. Fluid inclusions in magnetite-apatite ore from a cooling magmatic system at El Laco, Chile. *GFF* **1999**, *121*, 253–267. [CrossRef]
72. Ohmoto, H. Systematics of Sulfur and Carbon Isotopes in Hydrothermal Ore Deposits. *Econ. Geol. Bull. Soc. Econ. Geol.* **1972**, *67*, 551–578. [CrossRef]
73. Liu, Y.-N. Mineralization of Luohe-Xiaobaozhuang Iron Deposit in the Lu-Zong Volcanic Basin. Ph.D. Thesis, Hefei University of Technology, Hefei, China, 2015.
74. Ohmoto, H.; Rye, R.O. Isotopes of sulfur and carbon. In *Geochemistry of hydrothermal Ore Deposits*, 2nd ed.; Barnes, H.L., Ed.; John Wiley and Sons: New York, NY, USA, 1979; Volume 10, pp. 509–576.
75. Wu, Q.-H.; Wang, H.-T.; LeMessurier, M.J. Sulfur isotope of the Dabaozhuang and Luohe iron deposits with an approach to their genesis. *Miner. Depos.* **1983**, *4*, 24–26.
76. Rouchy, J.M.; Camoin, G.; Casanova, J.; Deconinck, J.F. The Central Palaeo-Andean Basin of Bolivia (Potosi Area) during the Late Cretaceous and Early Tertiary: Reconstruction of Ancient Saline Lakes using Sedimentological, Paleoecological and Stable Isotope Records. *Palaeogeogr. Palaeoclimatol. Palaeoecol.* **1993**, *105*, 179–198. [CrossRef]
77. Chu, X.-L.; Chen, J.-S.; Wang, S.-X. Sulfur isotopic temperatures and their significance of Luohe iron deposit in Anhui Province. *Geochemical* **1984**, *13*, 350–356.
78. Lu, H.-Z.; Fan, H.-R.; Ni, P. *Fluid Inclusion*; Science Press: Beijing, China, 2004.
79. Bain, W.M.; Steele-MacInnis, M.; Li, K.; Li, L.; Mazdab, F.K.; Marsh, E.E. A fundamental role of carbonate–sulfate melts in the formation of iron oxide–apatite deposits. *Nat. Geosci.* **2020**, *13*, 751–757. [CrossRef]
80. Watson, E.B. Two-liquid partition coefficients: Experimental data and geochemical implications. *Contrib. Miner. Petrol.* **1976**, *56*, 119–134. [CrossRef]
81. Yuan, J.-Z. Iron ore types and genesis of Meishan iron ore deposit-the study of high temperature experiments. *Geoscience* **1990**, *4*, 77–84.
82. Hemley, J.J.; Cygan, G.L.; Fein, J.B.; Robinson, G.R.; d'Angelo, W.M. Hydrothermal Ore-Forming Processes in the Light of Studies in Rock-Buffered Systems; I, Iron-Copper-Zinc-Lead Sulfide Solubility Relations. *Econ. Geol. Bull. Soc. Econ. Geol.* **1992**, *87*, 1–22. [CrossRef]
83. Hou, T.; Charlier, B.; Holtz, F.; Veksler, I.; Zhang, Z.-C.; Thomas, R.; Namur, O. Immiscible hydrous Fe–Ca–P melt and the origin of iron oxide-apatite ore deposits. *Nat. Commun.* **2018**, *9*, 1415. [CrossRef] [PubMed]
84. Philpotts, A.R. Silicate liquid immiscibility in tholeiitic basalts. *J. Petrol.* **1979**, *20*, 99–118. [CrossRef]
85. Xie, Q.-H.; Zhang, Z.-C.; Campos, E.; Deng, J.; Cheng, Z.G.; Fei, X.H.; Ke, S. Constraints of Fe-O isotopes on the origin of magnetite in the El Laco Kiruna-type iron deposit, Chile. *Ore Geol. Rev.* **2021**, *130*, 103967. [CrossRef]
86. Velasco, F.; Tornos, F.; Hanchar, J.M. Immiscible iron- and silica-rich melts and magnetite geochemistry at the El Laco volcano (northern Chile): Evidence for a magmatic origin for the magnetite deposits. *Ore Geol. Rev.* **2016**, *79*, 346–366. [CrossRef]
87. Naslund, H.R. The Effect of Oxygen Fugacity on Liquid Immiscibility in Iron-Bearing Silicate Melts. *Am. J. Sci.* **1983**, *283*, 1034–1059. [CrossRef]
88. Snyder, D.; Carmichael, I.S.E.; Wiebe, R.A. Experimental Study of Liquid Evolution in an Fe-Rich, Layered Mafic Intrusion: Constraints of Fe-Ti Oxide Precipitation on the T-fO_2 and T-ρ Paths of Tholeiitic Magmas. *Contrib. Mineral. Petrol.* **1993**, *113*, 73–86. [CrossRef]